





Emergent axion response in multilayered metamaterials

Leon Shaposhnikov ¹, Maxim Mazanov ¹, Daniel A. Bobylev,¹ Frank Wilczek ^{2,3,4,5} and Maxim A. Gorlach ^{1,*}

¹*School of Physics and Engineering, ITMO University, Saint Petersburg 197101, Russia*

²*Department of Physics, Stockholm University, Stockholm 10691, Sweden*

³*Center for Theoretical Physics, Massachusetts Institute of Technology, Cambridge, Massachusetts 02139, USA*

⁴*Department of Physics, Arizona State University, Tempe, Arizona 25287, USA*

⁵*Wilczek Quantum Center, Department of Physics and Astronomy, Shanghai Jiao Tong University, Shanghai 200240, China*



(Received 13 February 2023; revised 21 June 2023; accepted 14 August 2023; published 1 September 2023)

We consider the design of metamaterials whose behavior embodies the equations of axion electrodynamics. We derive an effective medium description of an assembly of magneto-optical layers with out-of-plane magnetization analytically and show how to achieve effective axion response with tunable parameters. We display some key predictions and validate them numerically.

DOI: [10.1103/PhysRevB.108.115101](https://doi.org/10.1103/PhysRevB.108.115101)

I. INTRODUCTION

The composition of dark matter is a major open question in physics and cosmology [1]. Because, presently, we have only upper limits on nongravitational interactions of dark matter, while gravitation is a universal force, several kinds of particles could explain the origin of the dark matter [2]. Axions [3,4] are among the most intriguing possibilities because their existence is suggested on independent grounds and their predicted properties follow from deep conceptual principles.

An axion is anticipated to be a light particle, with masses in the range from μeV to meV being favored [5,6], although smaller masses are also possible. The predicted high phase-space density of cosmological axions allows them to be described by a classical pseudoscalar axion field. The electromagnetic coupling of this field leads to additional terms in the Maxwell equations in the form [7,8]

$$\text{rot}(\mu^{-1} \mathbf{B}) = \frac{1}{c} \frac{\partial(\varepsilon \mathbf{E})}{\partial t} + \frac{4\pi}{c} \mathbf{j} + \varkappa [\nabla \mathbf{a} \times \mathbf{E}] + \frac{\varkappa}{c} \frac{\partial \mathbf{a}}{\partial t} \mathbf{B}, \quad (1)$$

$$\text{div}(\varepsilon \mathbf{E}) = 4\pi \rho - \varkappa (\nabla \mathbf{a} \cdot \mathbf{B}), \quad (2)$$

$$\text{rot} \mathbf{E} = -\frac{1}{c} \frac{\partial \mathbf{B}}{\partial t}, \quad \text{div} \mathbf{B} = 0. \quad (3)$$

Here, ρ and \mathbf{j} are the conventional charges and currents, ε and μ are the permittivity and permeability of the background medium, and \varkappa is the axion coupling constant of the electromagnetic field.

If cosmic axions exist, their coupling constant \varkappa is extremely feeble, which makes their experimental observation

challenging. On the other hand, Eqs. (1)–(3) can be recast as Maxwell's equations in a medium:

$$\text{rot} \mathbf{H} = \frac{1}{c} \frac{\partial \mathbf{D}}{\partial t} + \frac{4\pi}{c} \mathbf{j}, \quad (4)$$

$$\text{div} \mathbf{D} = 4\pi \rho, \quad (5)$$

$$\text{rot} \mathbf{E} = -\frac{1}{c} \frac{\partial \mathbf{B}}{\partial t}, \quad \text{div} \mathbf{B} = 0, \quad (6)$$

where the constitutive relations take the form

$$\mathbf{D} = \varepsilon \mathbf{E} + \chi \mathbf{B}, \quad (7)$$

$$\mathbf{H} = -\chi \mathbf{E} + \mu^{-1} \mathbf{B}, \quad (8)$$

and $\chi = \varkappa \mathbf{a}$. Hence, if some material is described by the constitutive relations (7) and (8), its electromagnetic properties are precisely captured by the equations of axion electrodynamics, and it is said that the material features *an effective axion field*. The origin of this effective field is not related to cosmic axions.

Collective excitations that couple like $\mathbf{a}(x, t)$ are known as emergent axions [9–12]. More common are materials that support a nontrivial constant value of \mathbf{a} . Then the new phenomena arise primarily at interfaces and boundaries.

In condensed matter physics these sorts of constitutive relations occur in magnetoelectrics and multiferroics [13,14]. Such materials were predicted theoretically [15] and later found in nature, Cr_2O_3 being the first example, followed later by a large class of other magnetoelectric materials [13,14]. Multiferroics have received significant attention from the condensed matter community because they are of practical use, for instance, for e-ink technology in electronic books. However, the effective axion response of such structures is relatively weak ($\chi \approx 10^{-3} - 10^{-2}$) and requires low temperatures in some cases [14]. Strong three-dimensional topological insulators also feature a quantized effective axion response [11,16] that is manifested in some cases up to the optical frequencies [17].

*m.gorlach@metalab.ifmo.ru

Parallel investigations occurred in the macroscopic electromagnetism community. There, materials described by the constitutive relations (7) and (8) are known as *Tellegen media*, while χ is sometimes termed the Tellegen coefficient. Such materials were first considered by Tellegen, who suggested a medium consisting of electric and magnetic dipoles attached to each other [18]. Tellegen media as well as a wider class of bianisotropic materials were actively investigated [19,20], and examples of meta-atoms featuring an effective Tellegen response were put forward [21,22].

Metamaterials are artificially structured media with sub-wavelength periodicity and engineered, often unconventional, electromagnetic properties [23–27]. The area of metamaterials has led to such spectacular developments as negative refraction [28], subwavelength imaging [29], and invisibility cloaking [30,31]. Recently, it has been proposed that wire metamaterials [32–34] could be useful for cosmic axion detection [35].

In this paper we bring these strands together, introducing the concept of *axion metamaterials*. We demonstrate theoretically that multilayered structures [36–38] composed of conventional magneto-optical materials should provide practical axion metamaterials in the sense that they will obey the equations of axion electrodynamics to a good approximation over a substantial range of conditions. Notably, here, the axion response χ is a design parameter subject to flexible control. In particular, it need not be small and can reach values around 1 for realizations in the microwave and terahertz domains (see Appendix F). Qualitative understanding of the comparatively simple effective equations guides us to some distinctive physical predictions, which we validate quantitatively through numerical simulation of the full dynamics.

The remainder of this paper is organized as follows. In Sec. II, we discuss the suggested design of our axion metamaterial. Section III continues with the calculation of the effective axion response χ for the designed structure, revealing some unexpected aspects of metamaterial homogenization theory. In Sec. IV we examine spatial gradients of χ and obtain the equations of axion electrodynamics. Next, Sec. V discusses the ways to tailor and control the effective axion response of the designed metamaterial. In Sec. VI we validate our effective medium treatment by examining electromagnetic fields in the designed multilayered structure and comparing the results to those predicted by the effective medium model. Finally, we conclude our analysis by discussing the results and outlining future perspectives in Sec. VII.

II. DESIGN OF AXION METAMATERIAL AND SYMMETRY REQUIREMENTS

First, we examine the symmetry properties of the desired constitutive relations (7) and (8). Since \mathbf{E} and \mathbf{B} have different parities under spatial inversion \mathcal{P} , the effective axion response χ is odd under inversion, i.e., pseudoscalar. Due to the different behaviors of \mathbf{E} and \mathbf{B} under time reversal \mathcal{T} , χ is also \mathcal{T} odd. However, it remains invariant under the combined \mathcal{PT} transformation. Such behavior is fully consistent with that expected for an axion field. In an electromagnetic context, this response requires external fields breaking the reciprocity of the material.

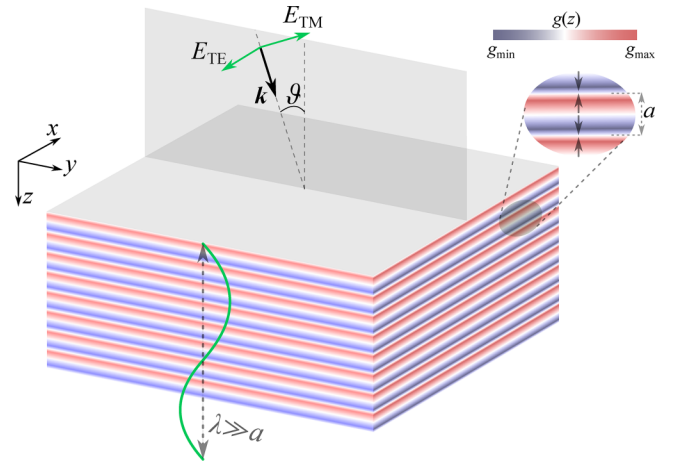


FIG. 1. Schematic of the designed multilayered structure composed of gyrotropic layers with spatially varying out-of-plane magnetization schematically shown by the black arrows. The average magnetization of the structure vanishes.

Furthermore, the constitutive relations (7) and (8) have a continuous rotational symmetry. To reconcile that with the fabrication capabilities, we require at least full rotational symmetry of the structure with respect to one axis, Oz .

As a simple structure fulfilling the above requirements we choose a multilayered metamaterial with out-of-plane magnetization of the layers parallel to the Oz axis (Fig. 1). To exclude the conventional magneto-optical effects such as the Faraday effect, we require average magnetization to be zero. The permittivity of a single layer is given by the expression

$$\hat{\varepsilon} = \begin{pmatrix} \varepsilon & i g(z) & 0 \\ -i g(z) & \varepsilon & 0 \\ 0 & 0 & \varepsilon \end{pmatrix}, \quad (9)$$

where $g(z)$ is a periodic function with period a , so that its Fourier expansion

$$g(z) = \sum_{n \neq 0} g_n e^{inbz}, \quad (10)$$

where $b = 2\pi/a$ is the reciprocal lattice period and $g_0 \equiv 0$ due to the vanishing average magnetization. From the symmetry point of view, the designed structure breaks time-reversal symmetry. However, the combination of spatial inversion and time reversal leaves it invariant, and there is a continuous rotational symmetry with respect to the z axis. Hence, the designed structure satisfies the necessary symmetry requirements.

It should be noted that the magnetoelectric response of antiferromagnetic structures has been known in condensed matter physics for a long time [14,15]. However, different magnetoelectrics feature a variety of electromagnetic phenomena which distinguish them from one another. A simple picture capturing their electrodynamics is currently lacking, while the ways to control and reconfigure their electromagnetic properties remain practically uncharted. To fill this gap, we investigate electrodynamics of the designed structure in detail, explicitly calculate the effective axion response,

estimate its typical values for several potential realizations, and show ways to control its magnitude.

III. EFFECTIVE AXION RESPONSE OF THE METAMATERIAL

The effective description of composite media relies on averaging rapidly oscillating local fields, which yields slowly varying *macroscopic fields*. The coefficients that relate the macroscopic polarization and magnetization to the averaged fields are associated with the effective material parameters [39]. The validity of the effective medium description is largely determined by the period-to-wavelength ratio, $\xi = a/\lambda$, which is considered to be small. The metamaterial homogenization strategy has been well established [40,41], with a history of application to various types of metamaterials [33,42], including multilayered ones [43–45]. Quite importantly, all homogenization approaches derive the effective material parameters from the bulk properties.

The current problem, however, has a subtle feature. Equations (1)–(3) suggest that an effective axion field which is constant in time and space does not modify Maxwell's equations. Therefore, analysis of the bulk properties in such a setting does not allow one to extract the Tellegen coefficient χ . Below, we prove that an analysis of the boundary conditions allows one to solve this problem, eventually yielding the equations of axion electrodynamics.

Using the periodicity of the structure, the fields in the metamaterial can be presented in the form

$$\begin{pmatrix} \mathbf{E}(\mathbf{r}) \\ \mathbf{D}(\mathbf{r}) \\ \mathbf{B}(\mathbf{r}) \end{pmatrix} = \sum_{n=-\infty}^{\infty} \begin{pmatrix} \mathbf{E}_n(\mathbf{r}) \\ \mathbf{D}_n(\mathbf{r}) \\ \mathbf{B}_n(\mathbf{r}) \end{pmatrix} e^{i\mathbf{k}^{(n)} \cdot \mathbf{r}}, \quad (11)$$

where the monochromatic $e^{-i\omega t}$ time dependence is suppressed throughout, $\mathbf{k}^{(n)} = (k_x, 0, k_z + nb)$, k_z and k_x are the components of the Bloch wave vector normal and parallel to the layers, respectively, and k_y can always be set to zero by the choice of the coordinate system. Here, \mathbf{E}_0 , \mathbf{D}_0 , and \mathbf{B}_0 are the respective averaged (or macroscopic) fields, while \mathbf{E}_n , \mathbf{D}_n , and \mathbf{B}_n , with nonzero n , are the amplitudes of the rapidly oscillating Floquet harmonics. In the analysis below, our goal is to derive the equations for the macroscopic fields excluding all rapidly oscillating terms.

The microscopic (nonaveraged) fields in the structure satisfy the conventional Maxwell's equations, which can be recast in the form

$$\nabla(\text{div } \mathbf{E}) - \Delta \mathbf{E} = q^2 \mathbf{D} + \frac{4\pi i q}{c} \mathbf{j}, \quad (12)$$

$$\text{div } \mathbf{D} = 0, \quad (13)$$

where $q = \omega/c$ and $\mathbf{j} = \mathbf{j}_0 e^{ik_x x + ik_z z}$ are the external distributed currents exciting the structure. The electric displacement for gyrotropic layers takes the form

$$\mathbf{D} = \varepsilon \mathbf{E} - ig(z) [\mathbf{e}_z \times \mathbf{E}]. \quad (14)$$

Substituting Floquet expansions for the fields [Eq. (11)] and Fourier series for the gyrotropy [Eq. (10)] in Eqs. (12)–(14), we recover the set of linear equations that relate the amplitudes of the Floquet harmonics. Applying perturbation theory

with a small $\xi = a/\lambda = q/b$, we derive the expressions for the Floquet harmonics of the electric field with $n \neq 0$ (see Appendix A):

$$E_{nx} = \frac{ig_n}{n^2 b^2} \left(q^2 - \frac{k_x^2}{\varepsilon} \right) E_{0y} + O(\xi^3), \quad (15)$$

$$E_{ny} = -ig_n \frac{q^2}{n^2 b^2} E_{0x} + O(\xi^3), \quad (16)$$

$$E_{nz} = -ig_n \frac{k_x}{\varepsilon n b} \left(1 - \frac{k_z}{nb} \right) E_{0y} + O(\xi^3). \quad (17)$$

Using the equation $\mathbf{B} = -i/q \text{rot } \mathbf{E}$, we can also evaluate the respective Floquet harmonics of the magnetic field as $\mathbf{B}_n = \mathbf{k}^{(n)} \times \mathbf{E}_n/q$. This yields

$$B_{nx} = ig_n \frac{q}{nb} E_{0x} + O(\xi^2), \quad (18)$$

$$B_{ny} = ig_n \frac{q}{nb} E_{0y} + O(\xi^2), \quad (19)$$

$$B_{nz} = -ig_n \frac{k_x q}{n^2 b^2} E_{0x} + O(\xi^3), \quad (20)$$

$$B_{0z} = \frac{k_x E_{0y}}{q}. \quad (21)$$

Having the explicit expressions for \mathbf{E}_n and \mathbf{B}_n , we now analyze the boundary conditions at the interface of the metamaterial with air. Clearly, the microscopic fields satisfy the conventional continuity conditions at the interface:

$$\mathbf{E}_t|_{z=0} = \mathbf{E}_t^{\text{out}}, \quad (22)$$

$$B_z|_{z=0} = B_z^{\text{out}}, \quad (23)$$

$$\mathbf{B}_t|_{z=0} = \mathbf{B}_t^{\text{out}}, \quad (24)$$

$$\varepsilon E_z|_{z=0} = E_z^{\text{out}}. \quad (25)$$

However, the microscopic field at the boundary of a metamaterial $z = 0$, $\mathbf{E}|_{z=0} = \sum_n \mathbf{E}_n$, is generally different from the averaged field \mathbf{E}_0 due to the contribution of higher-order Floquet harmonics. Keeping the terms up to the first power in small ξ and using the expressions for the Floquet harmonics above, we recover the following set of boundary conditions for the averaged fields:

$$\mathbf{E}_{0t} = \mathbf{E}_t^{\text{out}}, \quad \mathbf{B}_{0t} - \mathbf{B}_t^{\text{out}} = \chi \mathbf{E}_{0t}, \quad (26)$$

$$B_{0z} = B_z^{\text{out}}, \quad \varepsilon E_{0z} - E_z^{\text{out}} = -\chi B_{0z}. \quad (27)$$

Interestingly, we observe that the tangential components of \mathbf{B}_0 and normal components of $\varepsilon \mathbf{E}_0$ feature the discontinuity. As we prove below, these jumps in the averaged fields at the boundary are a signature of the Tellegen medium, and the coefficient χ quantifies the strength of the effective axion response:

$$\chi = -\frac{iq}{b} \sum_{n \neq 0} \frac{g_n}{n}. \quad (28)$$

It should be emphasized that the outlined picture of the effective Tellegen medium is valid once the metamaterial is subwavelength ($\xi = a/\lambda \ll 1$) and effects of the order of ξ^2 can be neglected. Counterintuitively, the effective Tellegen

response is fully isotropic even though the designed metamaterial has a single axis of continuous rotational symmetry and other rotational axes are lacking. Therefore, the developed description of the metamaterial holds for arbitrary incidence angles. However, as we discuss in Appendix B, the anisotropy in the electromagnetic response of our metamaterial arises in the second order in the period-to-wavelength ratio ξ .

Another interesting feature of our system is the dependence of χ on the structure termination. Indeed, if the boundary is shifted by Δ , the Fourier harmonics of gyrotropy $g(z)$ change from g_n to $g_n e^{inb\Delta}$. In the general case, this alters the effective axion response (28). This feature is in stark contrast to the behavior of the conventional material parameters, which are normally derived from the bulk properties and do not depend on the structure termination [40,41,45].

IV. SPATIAL GRADIENTS OF THE EFFECTIVE AXION RESPONSE

In the analysis above, we assumed that the metamaterial is periodic and time independent, which ensures constant χ . To demonstrate the link with axion electrodynamics and prove that χ is, indeed, the effective axion response, we generalize our treatment to the case of χ slowly varying in space, which mimics the so-called axion wind scenario [46]. For our metamaterial, this can be achieved by breaking the strict periodicity of the structure. To investigate this scenario, we divide the system into blocks with a characteristic size L much larger than the period of metamaterial a but smaller than the characteristic scale of χ variation (Fig. 2).

Applying Eqs. (26) and (27) to the boundary of the two adjacent blocks with χ_1 and χ_2 Tellegen coefficients, we recover the following discontinuities in \mathbf{B}_t and εE_z :

$$\begin{aligned} \mathbf{B}_{2t} - \mathbf{B}_{1t} &= (\chi_2 - \chi_1) \mathbf{E}_t, \\ \varepsilon E_{2z} - \varepsilon E_{1z} &= -(\chi_2 - \chi_1) B_z. \end{aligned}$$

On the other hand, such discontinuities result in the surface currents \mathbf{j}_s and charges ρ_s induced at the boundary between the blocks:

$$\begin{aligned} \frac{4\pi}{c} \mathbf{j}_s &= \mathbf{e}_z \times [\mathbf{B}_2 - \mathbf{B}_1] = (\chi_2 - \chi_1) [\mathbf{e}_z \times \mathbf{E}], \\ 4\pi \rho_s &= \varepsilon E_{2z} - \varepsilon E_{1z} = -(\chi_2 - \chi_1) B_z. \end{aligned}$$

To average the obtained distribution of the sources over scales of the order of L , we make the replacement $\mathbf{j}_s/L \rightarrow \mathbf{j}$, $\rho_s/L \rightarrow$

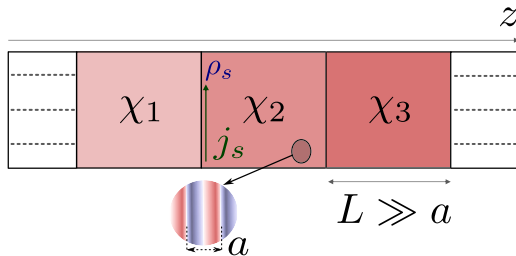


FIG. 2. Sketch of the metamaterial with broken strict periodicity, which is constructed of blocks with close values of χ . The boundaries between the blocks host surface charge with density ρ_s and surface current with density \mathbf{j}_s .

ρ , and $(\chi_2 - \chi_1)\mathbf{e}_z/L \rightarrow \nabla\chi$, where \mathbf{j} and ρ are the respective bulk currents and charges induced due to the gradient of the effective axion response. This procedure yields

$$\frac{4\pi}{c} \mathbf{j} = [\nabla\chi \times \mathbf{E}], \quad (29)$$

$$4\pi\rho = -\nabla\chi \cdot \mathbf{B}. \quad (30)$$

Inserting the obtained expressions into Maxwell's equations with sources, we obtain

$$\text{rot } \mathbf{B} = \frac{1}{c} \frac{\partial}{\partial t} (\varepsilon \mathbf{E}) + [\nabla\chi \times \mathbf{E}], \quad (31)$$

$$\text{div } (\varepsilon \mathbf{E}) = -\nabla\chi \cdot \mathbf{B}, \quad (32)$$

$$\text{rot } \mathbf{E} = -\frac{1}{c} \frac{\partial \mathbf{B}}{\partial t}, \quad \text{div } \mathbf{B} = 0. \quad (33)$$

In the case of time-independent χ , this matches the equations of axion electrodynamics (1)–(3), which allows us to interpret χ as an effective axion response.

V. TAILORING THE EFFECTIVE AXION RESPONSE

A unique advantage of the metamaterial platform is the possibility of tailoring the effective axion response χ on demand by manipulating the distribution of the magnetization and associated gyrotropy $g(z)$. As discussed in Sec. III, a counterintuitive, but technically straightforward, way to modify the axion response is to change the termination of the metamaterial. This potentially allows us not only to change the magnitude but also to swap the sign of χ .

Yet another approach is to tailor the spatial dependence of $g(z)$. To illustrate the dependence of the effective axion response on the functional form of $g(z)$, we recast the expression for χ in Eq. (28) in the form

$$\chi = \alpha_g M \frac{a}{\lambda}, \quad (34)$$

where $M = \max g(z)$ is the maximal gyrotropy within the unit cell, $\xi = a/\lambda = q/b$ is the period-to-wavelength ratio, and α_g is the dimensionless coefficient that depends on the specific form of the $g(z)$ function:

$$\alpha_g = \frac{1}{a} \int_0^a (\pi - bz) \tilde{g}(z) dz, \quad (35)$$

where $\tilde{g}(z) = g(z)/M$ (see the derivation in Appendix C). We examine several representative scenarios of the magnetization distribution within the unit cell (Fig. 3) with the same value of the maximal gyrotropy M . In each case, we evaluate the dimensionless α_g factor which quantifies the relative strength of the effective axion response at a given period-to-wavelength ratio a/λ . Comparing the step function with several other representative examples, including the harmonic magnetization modulation, we observe that the stepwise gyrotropy distribution maximizes the strength of the effective axion response.

To elaborate more on this observation, we explicitly derive an upper bound on α_g for fixed M and a/λ :

$$|\alpha_g| = \left| \frac{1}{a} \int_0^a (\pi - bz) \tilde{g}(z) dz \right| \leq \frac{1}{a} \int_0^a |\pi - bz| dz = \frac{\pi}{2}, \quad (36)$$

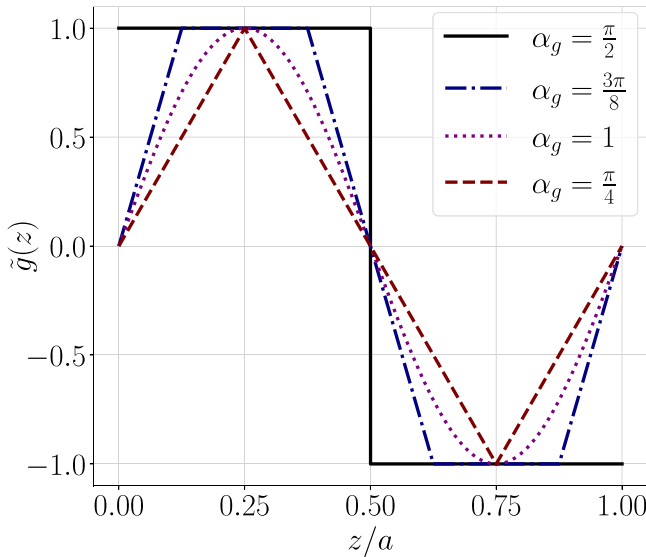


FIG. 3. Different spatial distributions of gyrotropy $\tilde{g}(z)$ within the unit cell, giving rise to the distinct values of the effective axion response in the metamaterial $\chi \propto \alpha_g$.

where we use the fact that $|\tilde{g}(z)| \leq 1$. Since $|(\pi - bz)| = (\pi - bz) \text{sgn}(\pi - bz)$, the upper limit $\alpha_g^{\max} = \pi/2$ is achieved when $\tilde{g} = \text{sgn}(\pi - bz)$, which is exactly the step-function profile. In this case, the maximal value of the effective axion response reads

$$\chi^{\max} = \frac{\pi}{2} M \frac{a}{\lambda}. \quad (37)$$

VI. VALIDATION OF THE EFFECTIVE MEDIUM DESCRIPTION

After deriving the effective medium picture of the designed metamaterial, we validate this approximate description. For that purpose, we simulate the behavior of the axion metamaterial with the stepwise gyrotropy distribution using the transfer matrix approach [47–49] or full wave numerical techniques that fully account for the metamaterial microstructure. The obtained results are compared to the predictions of the effective medium model with the effective axion response given by Eq. (37).

First, we examine the reflection of the plane wave at normal incidence from the finite slab of the axion metamaterial. Evaluating the effective axion response from Eq. (37) and employing the analytical theory of Tellegen media [50], we derive the electric field of the reflected wave $\mathbf{E}^r = \hat{r} \mathbf{E}^{\text{in}}$ with a 2×2 matrix \hat{r} having the components

$$r_{xx} = r_{yy} = -\frac{(\chi^2 + \varepsilon - \varepsilon_0) \sin \tilde{L}}{(\chi^2 + \varepsilon + \varepsilon_0) \sin \tilde{L} + 2i\sqrt{\varepsilon\varepsilon_0} \cos \tilde{L}}, \quad (38)$$

$$r_{xy} = -r_{yx} = \frac{2\chi\sqrt{\varepsilon_0} \sin \tilde{L}}{(\chi^2 + \varepsilon + \varepsilon_0) \sin \tilde{L} + 2i\sqrt{\varepsilon\varepsilon_0} \cos \tilde{L}}, \quad (39)$$

where $\tilde{L} = 2\pi\sqrt{\varepsilon}L/\lambda_0 = 2\sqrt{\varepsilon}\pi Na/\lambda_0$ is the optical path inside the slab, L is the thickness of the slab, N is the number of periods in the structure, λ_0 is the wavelength in vacuum, and ε and ε_0 are the permittivities of the Tellegen medium and host material, respectively. Thus, the polarization plane of the reflected light is rotated, and the reflected light contains both

copolarized and cross-polarized components proportional to r_{xx} and r_{yx} , respectively.

As expected, the major contribution to the copolarized reflectance comes from the difference between ε and ε_0 . Therefore, to isolate the contributions stemming from the effective axion response χ , we compare the results of the transfer matrix method to the analytical expressions (38) and (39) for the scenario $\varepsilon = \varepsilon_0$ for both cross-polarized [Fig. 4(a)] and copolarized [Fig. 4(b)] reflection coefficients. Assuming fixed thickness of the slab $L = 100a$, we gradually change the frequency of the incident wave, thus varying the period-to-wavelength ratio $\xi = a/\lambda$. If the metamaterial unit cell is deeply subwavelength ($\xi < 0.15$), the two approaches perfectly agree, with a typical discrepancy between them of the order of a few percent. However, a further increase of ξ results in significant errors that reach 50% for $\xi = 0.3$ that make the effective medium treatment inadequate.

To further check the validity of our model for plane wave propagation, we fix a sufficiently small period-to-wavelength ratio $\xi = 0.02$ and analyze the scenario with a nonzero incidence angle ϑ . Figure 4(c) compares the results calculated using the transfer matrix method [48] and those obtained from the effective medium approach. In the latter case, we evaluate the transfer matrix for the entire slab while employing the relevant boundary conditions and using the fact that the eigenmodes in the medium with axion response are degenerate and have a refractive index $n = \sqrt{\varepsilon\mu}$. Interestingly, we observe perfect agreement between the two approaches even for the large incidence angles approaching $\pi/2$. This highlights the isotropic nature of the effective axion response even though our model has only one axis of continuous rotational symmetry.

Next, we verify that the equations of axion electrodynamics (31)–(33) capture the behavior of our metamaterial once its periodicity is broken and a gradient of the effective axion response is introduced. For simplicity, we examine the case of a constant gradient that corresponds to Weyl semimetals [51–55], providing an instance of the so-called Carroll-Field-Jackiw electrodynamics [56].

A specific prediction of axion electrodynamics in this case is the rotation of the polarization plane of light [57], similar to the Faraday effect in magneto-optical materials. To verify this, we simulate the scenario of normal incidence while introducing a linear gradient of axion response $\chi(z) = \chi_{\max}z/L$, where L is the total thickness of the slab. The metamaterial slab is constructed from $N_b \gg 1$ blocks, each comprising N_l identical bilayers of subwavelength thickness $a \ll \lambda$, with each bilayer consisting of two layers having the same magnitude but opposite orientations of magnetization. The absolute value of magnetization is constant within each block but linearly changes throughout the blocks, which thus creates an approximation of the linear gradient of $\chi(z)$. The chosen parameters ensure that the spatial variation of the effective axion field is smooth. We compute the field in the metamaterial close to the output facet and average the field polarization over the block of $N_l \sim 10^2$ layers to exclude rapid oscillations at the subwavelength scale (see Appendix D). Figure 4(d) shows a comparison of transfer matrix results averaged in the described way with the effective medium picture, which suggests polarization rotation $\theta = \chi_{\max}/2$. The agreement

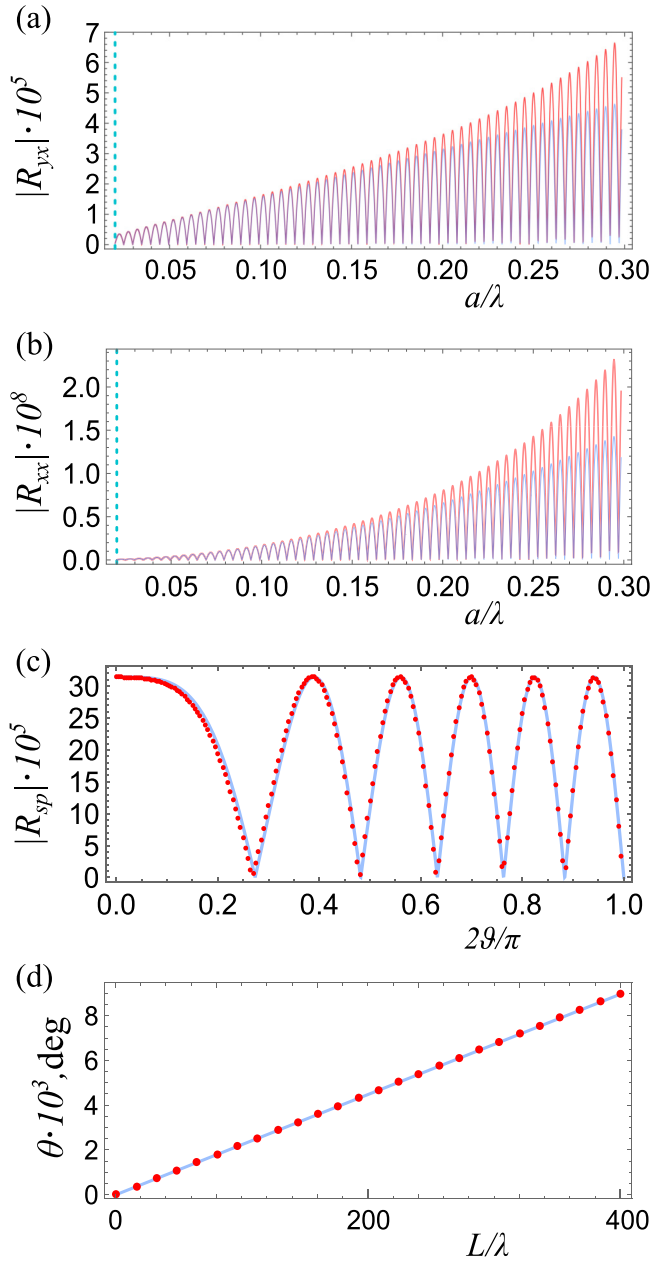


FIG. 4. Validation of the effective medium picture for the designed axion metamaterial with the stepwise gyrotropy distribution. Red lines and dots show the results of the transfer matrix method; light blue lines are the results of the effective medium approximation. (a) Cross-polarized and (b) copolarized reflection coefficients $|r_{yx}|$ and $|r_{xx}|$ for the slab versus the period-to-wavelength ratio a/λ . Vertical cyan dashed lines mark the ratio $a/\lambda = 1/50$ used in the calculations in (c) and (d). (c) Cross-polarized reflection coefficients $|R_{sp}| = |R_{ps}|$ for the slab of the axion metamaterial versus the incidence angle ϑ . (d) Averaged rotation angle of the microscopic field near the output facet of the axion metamaterial slab with a constant gradient of χ . Parameters of the simulations: $\varepsilon_0 = \varepsilon = 1$ and (a) and (b) $L = 100a$, $g = 0.01$; (c) $g = 0.01$, $L = 2.75\lambda$; and (d) $g_{\max} = 0.01L/(400\lambda)$.

between the two approaches is excellent for various thicknesses L of the slab, which confirms the validity of the effective medium description of inhomogeneous axion metamaterials.

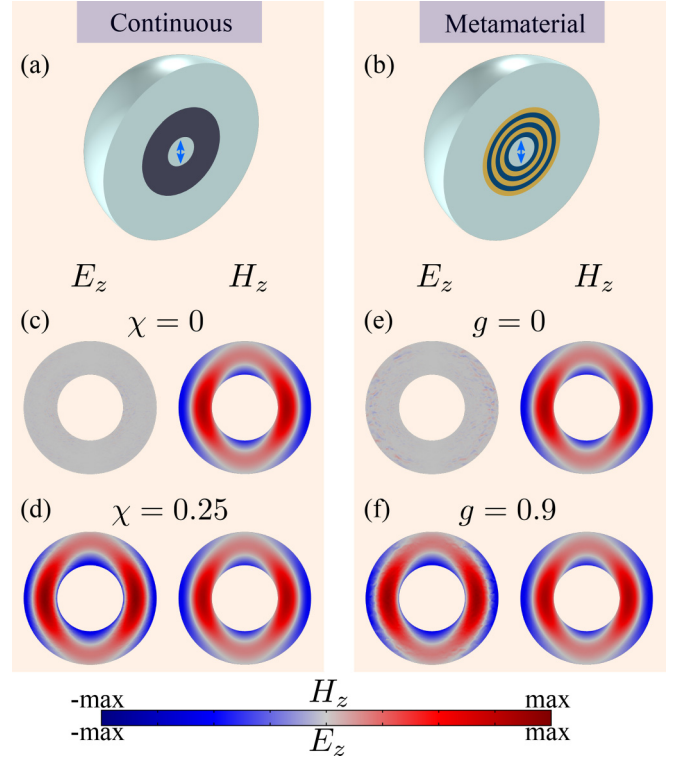


FIG. 5. Emergence of the electric dipole field for a point magnetic dipole inside the axion spherical shell. (a) and (b) Sketches of the simulated systems. (a) corresponds to the case of the continuous Tellegen medium ($\varepsilon = 1$, $\mu = 1$), whereas (b) shows the metamaterial realization with $\varepsilon = 1$ and $\mu = 1$. The blue arrows represent the point magnetic dipole oscillating with frequency $f = 1.0$ GHz. The distance from the dipole to the shell inner boundary is $\lambda/4$; the shell thickness is $\lambda/2$. The period of the layered structure is $a = \lambda/6$. Fields corresponding to (c) and (d) the continuous medium and (e) and (f) layered metamaterial when the effective axion response is either (c) and (e) zero or (d) and (f) nonzero.

Finally, we examine whether the effective medium treatment remains adequate when the metamaterial is excited by the external sources. To that end, we explore a dynamic analog of the Witten effect [58], which manifests as the emergence of an electric charge induced by the magnetic monopole placed inside an axion medium. In the condensed matter context, this effect was predicted to occur in axion topological insulators [59,60]. Below, we analyze the fields produced by the oscillating point magnetic dipole surrounded by an axion shell [Fig. 5(a)]. The theory [8] predicts that the axion shell hybridizes electric and magnetic responses such that the field outside is a superposition of magnetic and electric dipole fields [Figs. 5(c) and 5(d)]. To validate this physics, we simulate the magnetic dipole inside the designed metamaterial [Fig. 5(b)] and analyze scenarios with layer magnetization from zero [Fig. 5(e)] to some fixed nonzero value [Fig. 5(f)] matching the magnitude of ξ used in the effective medium calculation. Examining the obtained field patterns [Fig. 5(f)], we discover that our metamaterial indeed generates an electric dipole field with the induced electric dipole parallel to the magnetic one. Interestingly, the oscillating electric dipole inside the axion shell also induces an effective collinear magnetic moment, as further discussed in Appendix E.

VII. DISCUSSION AND CONCLUSIONS

We have proposed a practical design for an axion metamaterial and calculated its effective Tellegen response χ from first principles. While the building blocks of our metamaterial are conventional magneto-optical layers, an axion response for the entire structure emerges through their combined action. Our estimates showed that the designed structure may exhibit a strong effective axion response $\chi \approx 1$ in microwave and terahertz domains, providing a tabletop platform to test the effects of axion electrodynamics.

Interestingly, the strength of the axion response depends on the structure termination, which in turn affects the boundary conditions. The importance of boundary terms is well appreciated in the emergent axion theory but represents an important subtlety in metamaterial homogenization.

Our derivation of the effective axion response complements the existing tool kit of more abstract theoretical methods such as dimensional reduction procedures [9] and analysis of quantum field theory anomalies [61,62].

While the condensed matter community has been studying magnetoelectric and multiferroic materials for a long time, connecting them to metamaterials opens new pathways. The dual possibilities of producing metamaterials with corresponding properties but on larger length scales and with tunable properties or of “scaling up” to different kinds of metamaterials using magnetoelectric and multiferroic building blocks both deserve much further attention. Another promising possibility is achieving time-dependent control of χ , which potentially can be harnessed for cosmic axion detection [63–66].

ACKNOWLEDGMENTS

We acknowledge T. Seidov, Dr. A. Millar, Prof. A. Kalashnikova, and Prof. P. Belov for valuable discussions. Theoretical models were supported by the Priority 2030 Federal Academic Leadership Program. Numerical simulations were supported by the Russian Science Foundation (Grant No. 21-79-10209). L.S., M.M., D.A.B., and M.A.G. acknowledge partial support from the Foundation for the Advancement of Theoretical Physics and Mathematics “Basis.”

APPENDIX A: FLOQUET HARMONICS OF ELECTRIC FIELD

This Appendix supplements the discussion in Sec. III and provides the derivation of electric field Floquet harmonics. The starting point of this derivation is the set of Eqs. (12)–(14). Using the Fourier expansion of gyrotropy and Floquet expansion of electromagnetic field, Eqs. (10) and (11), we derive the set of scalar equations for the respective Floquet harmonics:

$$(k_z^{(n)})^2 E_{nx} - k_x k_z^{(n)} E_{nz} = q^2 D_{nx}, \quad (\text{A1})$$

$$[k_x^2 + (k_z^{(n)})^2] E_{ny} = q^2 D_{ny}, \quad (\text{A2})$$

$$-k_x k_z^{(n)} E_{nx} + k_x^2 E_{nz} = q^2 D_{nz}, \quad (\text{A3})$$

$$k_x D_{nx} + k_z^{(n)} D_{nz} = 0, \quad (\text{A4})$$

$$D_{nx} = \varepsilon E_{nx} + i \sum_{n' \neq n} g_{n-n'} E_{n'y}, \quad (\text{A5})$$

$$D_{ny} = \varepsilon E_{ny} - i \sum_{n' \neq n} g_{n-n'} E_{n'x}, \quad (\text{A6})$$

$$D_{nz} = \varepsilon E_{nz}. \quad (\text{A7})$$

From this system of equations, we calculate E_{nx} , E_{ny} , and E_{nz} up to the second power in small $\xi = a/\lambda = q/b$.

Equation (A2) yields $E_{ny} \approx q^2/(n^2 b^2) D_{ny} + O(\xi^3)$. In turn, Eq. (A6) suggests $D_{ny} = -i g_n E_{0x} + O(\xi^2)$. Combining these two results, we find

$$E_{ny} = -i g_n \frac{q^2}{n^2 b^2} E_{0x} + O(\xi^3). \quad (\text{A8})$$

Next, Eq. (A5) yields $D_{nx} = i g_n E_{0y} + O(\xi^2)$, and Eq. (A4) allows us to calculate D_{nz} : $D_{nz} = -k_x/k_z^{(n)} D_{nx} = -i g_n k_x/(n b) [1 - k_z/(n b)] E_{0y} + O(\xi^3)$. Using Eq. (A7), we immediately evaluate

$$E_{nz} = -i g_n \frac{k_x}{\varepsilon n b} \left(1 - \frac{k_z}{n b}\right) E_{0y} + O(\xi^3). \quad (\text{A9})$$

Finally, we use Eq. (A1) to calculate E_{nx} via the already found D_{nx} and E_{nz} , which yields

$$E_{nx} = \frac{i g_n}{n^2 b^2} \left(q^2 - \frac{k_x^2}{\varepsilon}\right) E_{0y} + O(\xi^3). \quad (\text{A10})$$

Equations (A8)–(A10) define higher-order Floquet harmonics via averaged fields, which allows us to construct the effective description of the metamaterial in terms of the averaged fields.

APPENDIX B: EFFECTIVE PERMITTIVITY OF THE AXION METAMATERIAL

In Sec. III, we focused our attention on the derivation of the effective axion response χ . For completeness, we discuss here the derivation of the effective permittivity of the metamaterial ε^{eff} , keeping the terms up to ξ^2 . We start from Eq. (14), which can be recast in the form

$$\mathbf{D}_0 = \varepsilon \mathbf{E}_0 + i \sum_{n \neq 0} g_{-n} [\mathbf{E}_n \times \mathbf{e}_z].$$

Combining this with the expressions for \mathbf{E}_n Floquet harmonics, Eqs. (15)–(17), we get

$$\begin{pmatrix} D_{0x} \\ D_{0y} \\ D_{0z} \end{pmatrix} = \begin{pmatrix} \varepsilon_{xx}^{\text{eff}} & 0 & 0 \\ 0 & \varepsilon_{yy}^{\text{eff}} & 0 \\ 0 & 0 & \varepsilon_{zz}^{\text{eff}} \end{pmatrix} \begin{pmatrix} E_{0x} \\ E_{0y} \\ E_{0z} \end{pmatrix},$$

where the components of the effective permittivity tensor in the chosen coordinate system ($k_y = 0$) calculated with precision up to ξ^2 read

$$\varepsilon_{xx}^{\text{eff}} = \varepsilon + q^2 \sum_{n \neq 0} \frac{g_n g_{-n}}{n^2 b^2}, \quad (\text{B1})$$

$$\varepsilon_{yy}^{\text{eff}} = \varepsilon + \left(q^2 - \frac{k_x^2}{\varepsilon}\right) \sum_{n \neq 0} \frac{g_n g_{-n}}{n^2 b^2}. \quad (\text{B2})$$

$$\varepsilon_{zz}^{\text{eff}} = \varepsilon. \quad (\text{B3})$$

We observe that the correction to the effective permittivity is of the order of ξ^2 , while the effective axion response χ is stronger, being of the order of ξ . Once terms proportional to ξ^2 are taken into account, the metamaterial becomes anisotropic, and spatial dispersion effects emerge. Note also that ε^{eff} does not depend on the choice of the unit cell as it is typical for the bulk properties of metamaterials [45]. In addition, the terms proportional to ξ^2 modify the boundary conditions.

$$\begin{aligned} -i \sum_{n \neq 0} \frac{g_n}{n} &= -i \sum_{n \neq 0} \frac{1}{na} \int_0^a g(z) e^{-inbz} dz = -\frac{i}{a} \int_0^a g(z) \left(\sum_{n \neq 0} \frac{e^{-inbz}}{n} \right) dz \\ &= -\frac{i}{a} \int_0^a g(z) [\ln(1 - e^{-ibz}) - \ln(1 - e^{ibz})] dz = \frac{1}{a} \int_0^a g(z) (\pi - bz) dz. \end{aligned} \quad (\text{C1})$$

Hence, the effective axion response can be recast in the form

$$\chi = \frac{1}{\lambda} \int_0^a g(z) (\pi - bz) dz. \quad (\text{C2})$$

APPENDIX D: DETAILS OF THE TRANSFER MATRIX METHOD

Here, we briefly discuss the calculation of the reflection and transmission coefficients, Faraday rotation, and ellipticity via the transfer matrix method at normal incidence, both for the case of isotropic Tellegen media and for the designed multilayered metamaterial. To examine oblique incidence, we use the general form of the transfer matrices derived in Ref. [48]. First, we discuss the application of the transfer matrix method to the calculation of transmission or reflection amplitudes under normal incidence in the homogeneous isotropic Tellegen medium described by the constitutive relations (7) and (8). The relevant amplitudes were calculated for some special cases of the homogeneous Tellegen media in Refs. [20,50], although using a different form of the material equations. As an amplitude column vector, we choose the four-component vector of tangential field components and define the transfer matrix \hat{M} as

$$\begin{pmatrix} \mathbf{E}(z) \\ \mathbf{e}_z \times \mathbf{B}(z) \end{pmatrix} = \hat{M} \begin{pmatrix} \mathbf{E}(0) \\ \mathbf{e}_z \times \mathbf{B}(0) \end{pmatrix}. \quad (\text{D1})$$

This choice of the basis is particularly convenient in view of the implementation of the relevant boundary condition, Eq. (26), which translates into a boundary transfer matrix between two isotropic Tellegen media with Tellegen parameters χ_1 and χ_2 :

$$\hat{M}_{1 \rightarrow 2} = \begin{pmatrix} \hat{I} & 0 \\ (\chi_2 - \chi_1) \hat{\mathbf{e}}_z^\times & \hat{I} \end{pmatrix}, \quad (\text{D2})$$

where \hat{I} is the two-dimensional unit matrix and the matrix

$$\hat{\mathbf{e}}_z^\times = \begin{pmatrix} 0 & -1 \\ 1 & 0 \end{pmatrix} \quad (\text{D3})$$

describes the effect of the vector product \mathbf{e}_z^\times on the transverse fields. Since the waves propagate in the bulk of the Tellegen medium identically to their propagation in an isotropic dielectric, the transfer matrix describing the bulk of the Tellegen

APPENDIX C: ANALYSIS OF THE FORMULA FOR THE EFFECTIVE AXION RESPONSE

In this Appendix, we rewrite the expression for the effective axion response χ [Eq. (28)] in a form more convenient for calculations. For that purpose, we transform the sum of the Fourier components g_n as follows:

medium coincides with that of a dielectric with the same permittivity ε and reads

$$\hat{M}_d(z) = \begin{pmatrix} \cos(kz) & -i \sin(kz)/\sqrt{\varepsilon} \\ -i \sin(kz)\sqrt{\varepsilon} & \cos(kz) \end{pmatrix}, \quad (\text{D4})$$

where $k = \sqrt{\varepsilon}\omega/c$. Hence, the full transfer matrix for the freestanding Tellegen slab of length L reads

$$\hat{M} = \hat{M}_{2 \rightarrow 1} \hat{M}_d(L) \hat{M}_{1 \rightarrow 2}. \quad (\text{D5})$$

Then, all the necessary reflection and transmission amplitudes can be deduced from the following system:

$$\begin{pmatrix} \mathbf{E}^r \\ -\sqrt{\varepsilon_0} \mathbf{E}^r \end{pmatrix} = \begin{pmatrix} \hat{M}_{11} & \hat{M}_{12} \\ \hat{M}_{21} & \hat{M}_{22} \end{pmatrix} \begin{pmatrix} \mathbf{E}^{\text{in}} + \mathbf{E}^r \\ -\sqrt{\varepsilon_0} \mathbf{E}^{\text{in}} + \sqrt{\varepsilon_0} \mathbf{E}^r \end{pmatrix} \quad (\text{D6})$$

where the superscript indices *in*, *t*, and *r* correspond to incident, transmitted, and reflected fields, respectively, and ε_0 is the permittivity of the medium surrounding the Tellegen slab. For example, the reflection matrix

$$\hat{R} = \begin{pmatrix} r_{xx} & r_{xy} \\ r_{yx} & r_{yy} \end{pmatrix} \quad (\text{D7})$$

connecting the incident and reflected fields ($\mathbf{E}^r = \hat{R} \mathbf{E}^{\text{in}}$) reads

$$\begin{aligned} \hat{R} &= -[\sqrt{\varepsilon_0} \hat{M}_{11} + \hat{M}_{21} + \varepsilon_0 \hat{M}_{12} + \sqrt{\varepsilon_0} \hat{M}_{22}]^{-1} \\ &\quad \times [\sqrt{\varepsilon_0} \hat{M}_{11} + \hat{M}_{21} - \varepsilon_0 \hat{M}_{12} - \sqrt{\varepsilon_0} \hat{M}_{22}], \end{aligned}$$

which yields Eqs. (38) and (39) in the main text. Second, we discuss the application of the transfer matrix method to the designed multilayered metamaterial. At normal incidence, boundary conditions for TM and TE modes coincide, and the modes with left and right circular polarizations (LCP and RCP) propagate without any mixing. Accordingly, we employ the exact transfer matrices in the basis of circular polarizations with amplitude vector $(E_{\rightarrow}^{\text{LCP}}, E_{\leftarrow}^{\text{LCP}}, E_{\rightarrow}^{\text{RCP}}, E_{\leftarrow}^{\text{RCP}})^T$, where the indices \leftarrow and \rightarrow indicate the direction of propagation of the corresponding plane waves, either along \mathbf{e}_z or in the opposite direction. The transfer matrix realizing the boundary

conditions between the two layers i and j then reads [47]

$$\hat{M}_{ij} = \frac{1}{2} \begin{pmatrix} 1 + \eta_{ij}^{\pm} & 1 - \eta_{ij}^{\pm} & 0 & 0 \\ 1 - \eta_{ij}^{\pm} & 1 + \eta_{ij}^{\pm} & 0 & 0 \\ 0 & 0 & 1 + \eta_{ij}^{\mp} & 1 - \eta_{ij}^{\mp} \\ 0 & 0 & 1 - \eta_{ij}^{\mp} & 1 + \eta_{ij}^{\mp} \end{pmatrix}, \quad (\text{D8})$$

where $\eta_{ij}^{\pm} = n_i^{\pm}/n_j^{\pm}$ and n_i^{\pm} are the refractive indices for LCP/RCP modes in the i th layer, which for layers with positive H_z read $n_{\pm}^{\pm} = \sqrt{\varepsilon_0 \pm g}$ and for layers with negative H_z read $n_{\pm}^{\pm} = \sqrt{\varepsilon_0 \mp g}$ (in air, $n_{\text{air}}^{\pm} = 1$). To model the perfect mirror, we use the boundary transfer matrix for the perfect electric conductor (PEC):

$$\hat{M}_{\text{PEC}} = \frac{1}{2} \begin{pmatrix} 1 & 1 & 0 & 0 \\ 1 & 1 & 0 & 0 \\ 0 & 0 & 1 & 1 \\ 0 & 0 & 1 & 1 \end{pmatrix}. \quad (\text{D9})$$

Transfer matrices describing the propagation in the bulk read

$$\hat{T}_i = \begin{pmatrix} e^{in_i^+ P} & 0 & 0 & 0 \\ 0 & e^{-in_i^+ P} & 0 & 0 \\ 0 & 0 & e^{in_i^- P} & 0 \\ 0 & 0 & 0 & e^{-in_i^- P} \end{pmatrix}, \quad (\text{D10})$$

where $P = 2\pi a/\lambda_0$, and λ_0 is the light wavelength in air. The resultant transfer matrix describing the entire multilayer with an even number ($2N$) of layers then reads

$$\hat{M}_{\text{AFM}} = \hat{M}_{\leftarrow \text{air}} \hat{M}_{\rightarrow \leftarrow} (\hat{M}_{\leftarrow \rightarrow} \hat{T}_{\leftarrow} \hat{M}_{\rightarrow \leftarrow} \hat{T}_{\rightarrow})^N \hat{M}_{\text{air} \rightarrow}, \quad (\text{D11})$$

while the transfer matrix for the same structure backed with a perfectly conducting mirror reads

$$\hat{M}_{\text{AFM+PEC}} = \hat{M}_{\text{PEC}} \hat{M}_{\leftarrow \text{air}}^{-1} \hat{M}_{\text{AFM}}. \quad (\text{D12})$$

Co- and cross-polarized reflection and transmission coefficients are then calculated as [47]

$$\begin{aligned} r_{xx} &= \frac{1}{2} \left(\frac{M_{2,1}}{M_{2,2}} + \frac{M_{4,3}}{M_{4,4}} \right), \quad r_{yx} = \frac{1}{2i} \left(\frac{M_{2,1}}{M_{2,2}} - \frac{M_{4,3}}{M_{4,4}} \right), \\ t_{xx} &= \frac{1}{2} \left(\frac{\det(\hat{M}_L)}{M_{2,2}} + \frac{\det(\hat{M}_R)}{M_{4,4}} \right), \\ t_{yx} &= \frac{1}{2i} \left(\frac{\det(\hat{M}_L)}{M_{2,2}} - \frac{\det(\hat{M}_R)}{M_{4,4}} \right), \end{aligned} \quad (\text{D13})$$

where \hat{M}_L and \hat{M}_R represent the upper left and lower right matrix blocks of the resultant transfer matrix, respectively. The angle of polarization rotation $\theta^{r,t}$ and ellipticity $\eta^{r,t}$ are calculated via

$$\begin{aligned} 2\theta^s &= \tan^{-1} \left(\frac{2\text{Re}(K_s)}{1 - |K_s|^2} \right), \\ 2\eta^s &= \sin^{-1} \left(\frac{2\text{Im}(K_s)}{1 + |K_s|^2} \right), \end{aligned} \quad (\text{D14})$$

where $K_s = s_{yx}/s_{xx}$ and $s \in \{r, t\}$. While the main text discusses the reflection from the freestanding slab of the axion metamaterial, we also compare numerical and analytical results for the reflection from the axion metamaterial backed by the ideal mirror. For that purpose, we employ the same

transfer matrix approach as above, but with a different full transfer matrix,

$$\hat{M}_{\text{PEC}} = \hat{M}_d(L) \hat{M}_{1 \rightarrow 2}, \quad (\text{D15})$$

while forcing the transmitted field \mathbf{E}^t in Eq. (D6) to vanish at the PEC boundary. This allows us to calculate the reflection amplitudes r_{xx} and r_{yx} and the rotation angle of the reflected light via Eq. (D14):

$$\theta^r = \frac{1}{2} \arctan \left[\frac{4\chi\psi\sqrt{\varepsilon_0}\sin^2\tilde{L}}{-4\chi^2\varepsilon_0\sin^4\tilde{L} + \psi^2} \right], \quad (\text{D16})$$

where $\psi = \varepsilon \cos^2\tilde{L} + \sin^2\tilde{L}(\varepsilon_0 - \chi^2)$ and the ellipticity of the reflected light vanishes. For the typical scenario $\chi \ll 1$, Eq. (D16) gives

$$\theta^r \approx \frac{2\chi\sqrt{\varepsilon_0}\sin^2\tilde{L}}{\varepsilon \cos^2\tilde{L} + \varepsilon_0 \sin^2\tilde{L}}. \quad (\text{D17})$$

This prediction is reproduced with high precision by the transfer matrix method (Fig. 6).

Note that while calculating the predictions of the effective medium model with precision up to χ^2 , we also have to take into account the corrections to the effective permittivity of the metamaterial that also are of the order of χ^2 (see Appendix B).

For the multilayered structure under study with $g_n = ig(e^{-i\pi n} - 1)/(\pi n)$, this correction reads $\Delta\varepsilon^{\text{eff}} \equiv (\varepsilon_{xx,yy}^{\text{eff}} - \varepsilon) = (a/\lambda)^2 g^2 (\pi^2/12)$. Using this value of the permittivity, $\varepsilon \rightarrow \varepsilon + \Delta\varepsilon^{\text{eff}}$, in Eqs. (38) and (39), we find that the calculated cross- and copolarized reflection coefficients r_{xy} and r_{xx} perfectly agree with the results of the transfer matrix approach [see Fig. 4(b)].

Finally, in order to calculate the average polarization of the field near the output facet of the multilayer with a linear gradient of the effective axion response, we compose such a multilayer out of $N_b \gg 1$ blocks of length L/N_b , where L is the total slab thickness, each comprising $N_l \gg L/(\lambda N_b)$ individual bilayers with the same magnitude but opposite orientation of magnetization. In this case, each block can be ascribed an effective Tellegen coefficient which differs from block to block, defining a spatially varying effective axion response $\chi(z)$. To calculate Fig. 4 in the main text, the following parameters are used: $N_b = 100$, $N_l = 200$, and $a = \lambda/50$.

APPENDIX E: POINT ELECTRIC DIPOLE INSIDE THE AXION METAMATERIAL

As discussed in the main text (Fig. 5), a point magnetic dipole surrounded by an axion spherical shell produces a combination of electric and magnetic dipole fields. A similar effect is observed if the point electric dipole is placed inside the axion shell [Figs. 7(a) and 7(b)]. In this case, the field outside the shell is expected to be a combination of collinear electric and magnetic dipoles [Fig. 5(d)]. This expectation is confirmed by the full-wave numerical simulations of the electric dipole inside the designed metamaterial [Fig. 5(f)], which highlights once again the validity of the effective medium description.

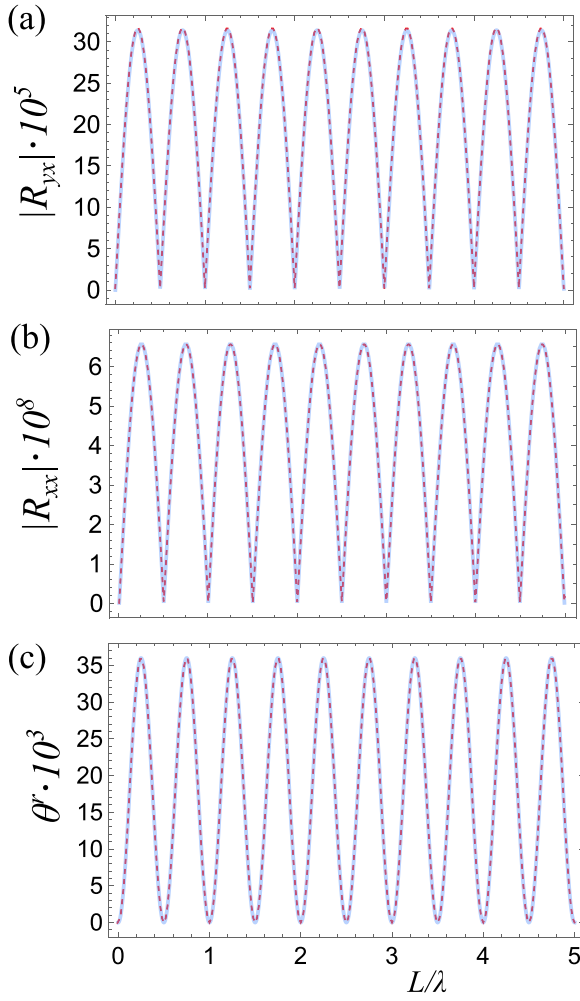


FIG. 6. Calculation of the reflection coefficient from the slab of the axion metamaterial backed by the ideal mirror. Blue solid and red dashed lines show the predictions of the effective medium approach and transfer matrix method, respectively. (a) and (b) Cross- and copolarized reflection coefficients versus the thickness L of the slab for the fixed period-to-wavelength ratio $a/\lambda = 0.02$. The effective medium results [Eq. (39)] include second-order corrections $\propto \chi^2$ to the effective permittivity. (c) Rotation of the polarization plane θ' for the light reflected from the mirror-coated axion metamaterial slab versus the total slab thickness L . Parameters: $a/\lambda = 0.02$, $\epsilon_0 = 1.0$, $g = 0.01$.

APPENDIX F: ESTIMATION OF THE AXION RESPONSE χ

Below, we estimate the effective axion response for two realizations in the terahertz and microwave domains showing that χ can reach very high values approaching 1. Importantly, in both cases the suggested structures can operate at room temperature. To minimize the demagnetizing effect of the adjacent layers on each other, dielectric spacers can be inserted between them.

To implement an effective axion response in the terahertz range (frequencies around 0.5 THz), we suggest exploiting thin HgTe films with a giant magneto-optical response [67]. Specifically, Faraday rotation in such films reaches $\pi/4$ at a

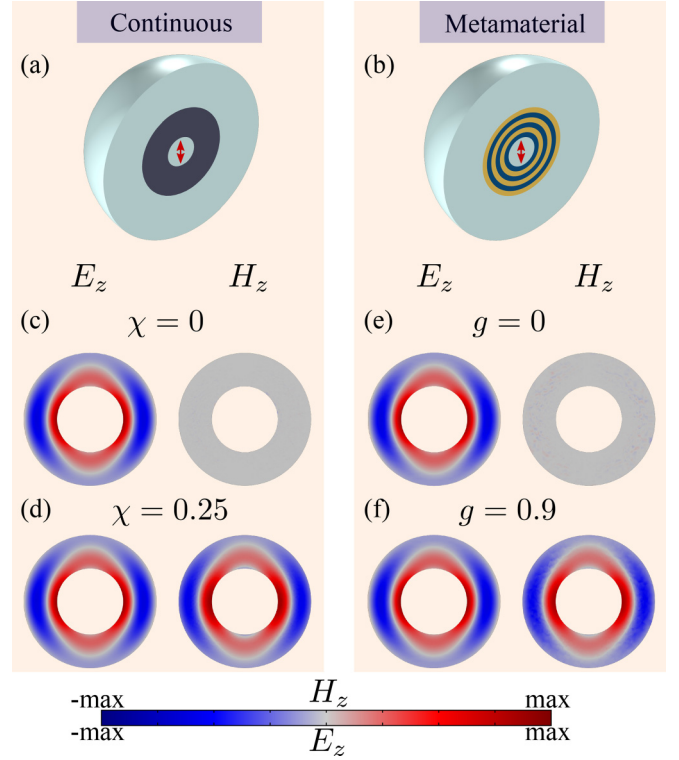


FIG. 7. Emergence of the magnetic dipole field for a point electric dipole inside an axion spherical shell. (a) and (b) Sketches of the simulated systems. (a) corresponds to the case of the continuous Tellegen medium ($\epsilon = 1$, $\mu = 1$), and (b) shows the metamaterial realization with $\epsilon = 1$ and $\mu = 1$. The red arrows represent the point electric dipole oscillating with frequency $f = 1.0$ GHz. The distance from the dipole to the shell inner boundary is $\lambda/4$; the shell thickness is $\lambda/2$. The period of the layered structure is $a = \lambda/6$. Fields corresponding to (c) and (d) the continuous medium and (e) and (f) layered metamaterial when the effective axion response is either (c) and (e) zero or (d) and (f) nonzero.

distance of $1 \mu\text{m}$ in 0.6 T magnetic field, which allows us to estimate the Verdet constant.

For estimation purposes, we assume the period-to-wavelength ratio $a = 1/7$, which is sufficient for the effective axion description to be valid, and magnetic field $B_0 = 0.1$ T, which is attainable in arrays of nanomagnets [68]. Next, we calculate the effective axion response from Eq. (37) estimating the gyrotropy value g from the Faraday rotation above. This yields χ of the order of unity.

In the microwave domain, a promising realization can be based on the gyrotropy of the permeability tensor arising in a class of ferrite materials. For instance, commercially available Ni-Zn ferrite compounds feature strong gyrotropy g , reaching 4 at frequencies close to 6 GHz [69]. Assuming the same period-to-wavelength ratio of $1/7$, we estimate the maximal χ to be also around 1.

Finally, it is also possible to exploit natural antiferromagnets by combining them with other materials to enhance the effective axion response. Thus, our proposal of an axion metamaterial makes it possible to engineer a strong and controllable effective axion response.

- [1] G. Bertone and D. Hooper, History of dark matter, *Rev. Mod. Phys.* **90**, 045002 (2018).
- [2] J. L. Feng, Dark matter candidates from particle physics and methods of detection, *Annu. Rev. Astron. Astrophys.* **48**, 495 (2010).
- [3] F. Wilczek, Problem of Strong P and T Invariance in the Presence of Instantons, *Phys. Rev. Lett.* **40**, 279 (1978).
- [4] S. Weinberg, A New Light Boson? *Phys. Rev. Lett.* **40**, 223 (1978).
- [5] V. B. Klaer and G. D. Moore, The dark-matter axion mass, *J. Cosmol. Astropart. Phys.* (2017) 049.
- [6] M. Buschmann, J. W. Foster, and B. R. Safdi, Early-Universe Simulations of the Cosmological Axion, *Phys. Rev. Lett.* **124**, 161103 (2020).
- [7] P. Sikivie, Experimental Tests of the “Invisible” Axion, *Phys. Rev. Lett.* **51**, 1415 (1983).
- [8] F. Wilczek, Two Applications of Axion Electrodynamics, *Phys. Rev. Lett.* **58**, 1799 (1987).
- [9] X.-L. Qi, T. L. Hughes, and S.-C. Zhang, Topological field theory of time-reversal invariant insulators, *Phys. Rev. B* **78**, 195424 (2008).
- [10] A. M. Essin, J. E. Moore, and D. Vanderbilt, Magnetoelectric Polarizability and Axion Electrodynamics in Crystalline Insulators, *Phys. Rev. Lett.* **102**, 146805 (2009).
- [11] D. M. Nenko, C. A. C. Garcia, J. Gooth, C. Felser, and P. Narang, Axion physics in condensed-matter systems, *Nat. Rev. Phys.* **2**, 682 (2020).
- [12] A. Sekine and K. Nomura, Axion electrodynamics in topological materials, *J. Appl. Phys.* **129**, 141101 (2021).
- [13] W. Eerenstein, N. D. Mathur, and J. F. Scott, Multiferroic and magnetoelectric materials, *Nature (London)* **442**, 759 (2006).
- [14] A. P. Pyatakov and A. K. Zvezdin, Magnetoelectric and multiferroic media, *Usp. Fiz. Nauk* **182**, 593 (2012).
- [15] I. E. Dzyaloshinskii, On the magneto-electrical effect in antiferromagnets, *Sov. Phys. JETP* **10**, 628 (1960).
- [16] L. Wu, M. Salehi, N. Koirala, J. Moon, S. Oh, and N. P. Armitage, Quantized Faraday and Kerr rotation and axion electrodynamics of a 3D topological insulator, *Science* **354**, 1124 (2016).
- [17] J. Ahn, S.-Y. Xu, and A. Vishwanath, Theory of optical axion electrodynamics and application to the Kerr effect in topological antiferromagnets, *Nat. Commun.* **13**, 7615 (2022).
- [18] B. D. H. Tellegen, The gyrator, a new electric network element, *Philips Res. Rep.* **3**, 81 (1948).
- [19] J. A. Kong, Optics of bianisotropic media, *J. Opt. Soc. Am.* **64**, 1304 (1974).
- [20] A. Serdyukov, I. Semchenko, S. Tretyakov, and A. Sihvola, *Electromagnetics of Bi-anisotropic Materials: Theory and Applications* (Gordon and Breach Science, Amsterdam, 2001).
- [21] S. A. Tretyakov, S. I. Maslovski, I. S. Nefedov, A. J. Viitanen, P. A. Belov, and A. Sanmartin, Artificial Tellegen particle, *Electromagnetics* **23**, 665 (2003).
- [22] V. S. Asadchy and S. A. Tretyakov, Modular Analysis of Arbitrary Dipolar Scatterers, *Phys. Rev. Appl.* **12**, 024059 (2019).
- [23] V. G. Veselago, The electrodynamics of substances with simultaneously negative values of ϵ and μ , *Sov. Phys. Usp.* **10**, 509 (1968).
- [24] G. V. Eleftheriades and K. G. Balmain, *Negative-Refraction Metamaterials: Fundamental Principles and Applications* (Wiley, Hoboken, NJ, 2005).
- [25] T. Itoh and C. Caloz, *Electromagnetic Metamaterials: Transmission Line Theory and Microwave Applications* (Wiley, Hoboken, NJ, 2005).
- [26] R. Marques, F. Martin, and M. Sorolla, *Metamaterials with Negative Parameters* (Wiley, Hoboken, NJ, 2008).
- [27] *Theory and Phenomena of Metamaterials*, edited by F. Capolino (CRC Press, New York, 2009).
- [28] D. R. Smith, W. J. Padilla, D. C. Vier, S. C. Nemat-Nasser, and S. Schultz, Composite Medium with Simultaneously Negative Permeability and Permittivity, *Phys. Rev. Lett.* **84**, 4184 (2000).
- [29] J. B. Pendry, Negative Refraction Makes a Perfect Lens, *Phys. Rev. Lett.* **85**, 3966 (2000).
- [30] U. Leonhardt, Optical conformal mapping, *Science* **312**, 1777 (2006).
- [31] J. B. Pendry, D. Schurig, and D. R. Smith, Controlling electromagnetic fields, *Science* **312**, 1780 (2006).
- [32] J. B. Pendry, A. J. Holden, D. J. Robbins, and W. J. Stewart, Low frequency plasmons in thin-wire structures, *J. Phys.: Condens. Matter* **10**, 4785 (1998).
- [33] P. A. Belov, R. Marqués, S. I. Maslovski, I. S. Nefedov, M. Silveirinha, C. R. Simovski, and S. A. Tretyakov, Strong spatial dispersion in wire media in the very large wavelength limit, *Phys. Rev. B* **67**, 113103 (2003).
- [34] C. R. Simovski, P. A. Belov, A. V. Atrashchenko, and Y. S. Kivshar, Wire Metamaterials: Physics and Applications, *Adv. Mater.* **24**, 4229 (2012).
- [35] M. Lawson, A. J. Millar, M. Pancaldi, E. Vitagliano, and F. Wilczek, Tunable Axion Plasma Haloscopes, *Phys. Rev. Lett.* **123**, 141802 (2019).
- [36] L. M. Brekhovskikh, *Waves in Layered Media* (Academic, New York, 1980).
- [37] P. Yeh, *Optical Waves in Layered Media* (Wiley, New York, 1988).
- [38] S. V. Zhukovsky, A. Andryieuski, O. Takayama, E. Shkondin, R. Malureanu, F. Jensen, and A. V. Lavrinenko, Experimental Demonstration of Effective Medium Approximation Breakdown in Deeply Subwavelength All-Dielectric Multilayers, *Phys. Rev. Lett.* **115**, 177402 (2015).
- [39] V. M. Agranovich and V. L. Ginzburg, *Crystal Optics with Spatial Dispersion and Excitons* (Springer, Berlin, 1984).
- [40] M. G. Silveirinha, Metamaterial homogenization approach with application to the characterization of microstructured composites with negative parameters, *Phys. Rev. B* **75**, 115104 (2007).
- [41] A. Alù, First-principles homogenization theory for periodic metamaterials, *Phys. Rev. B* **84**, 075153 (2011).
- [42] M. G. Silveirinha, Generalized Lorentz-Lorenz formulas for microstructured materials, *Phys. Rev. B* **76**, 245117 (2007).
- [43] A. V. Chebykin, A. A. Orlov, A. V. Vozianova, S. I. Maslovski, Y. S. Kivshar, and P. A. Belov, Nonlocal effective medium model for multilayered metal-dielectric metamaterials, *Phys. Rev. B* **84**, 115438 (2011).
- [44] C. Rizza, V. Galdi, and A. Ciattoni, Enhancement and interplay of first- and second-order spatial dispersion in metamaterials with moderate-permittivity inclusions, *Phys. Rev. B* **96**, 081113(R) (2017).
- [45] M. A. Goriach and M. Lapine, Boundary conditions for the effective-medium description of subwavelength multilayered structures, *Phys. Rev. B* **101**, 075127 (2020).

- [46] I. G. Irastorza and J. Redondo, New experimental approaches in the search for axion-like particles, *Prog. Part. Nucl. Phys.* **102**, 89 (2018).
- [47] P. Markos and C. Soukoulis, *Wave Propagation: From Electrons to Photonic Crystals and Left-Handed Materials* (Princeton University Press, Princeton, NJ, 2008).
- [48] J. Zak, E. R. Moog, C. Liu, and S. D. Bader, Universal approach to magneto-optics, *J. Magn. Magn. Mater.* **89**, 107 (1990).
- [49] M. Born and E. Wolf, *Principles of Optics: Electromagnetic Theory of Propagation, Interference and Diffraction of Light* (Cambridge University Press, Cambridge, 1999).
- [50] I. V. Lindell, A. H. Sihvola, S. Tretyakov, and A. J. Viitanen, *Electromagnetic Waves in Chiral and Bi-isotropic Media* (Artech House, London, 1994).
- [51] A. G. Grushin, Consequences of a condensed matter realization of Lorentz-violating QED in Weyl semi-metals, *Phys. Rev. D* **86**, 045001 (2012).
- [52] A. A. Zyuzin and A. A. Burkov, Topological response in Weyl semimetals and the chiral anomaly, *Phys. Rev. B* **86**, 115133 (2012).
- [53] C. Guo, V. S. Asadchy, B. Zhao, and S. Fan, Light control with Weyl semimetals, *eLight* **3**, 2 (2023).
- [54] B. Zhao, C. Guo, C. A. C. Garcia, P. Narang, and S. Fan, Axion-field-enabled nonreciprocal thermal radiation in Weyl semimetals, *Nano Lett.* **20**, 1923 (2020).
- [55] V. S. Asadchy, C. Guo, B. Zhao, and S. Fan, Sub-wavelength passive optical isolators using photonic structures based on Weyl semimetals, *Adv. Opt. Mater.* **8**, 2000100 (2020).
- [56] S. M. Carroll, G. B. Field, and R. Jackiw, Limits on a Lorentz- and parity-violating modification of electrodynamics, *Phys. Rev. D* **41**, 1231 (1990).
- [57] D. Harari and P. Sikivie, Effects of a Nambu-Goldstone Boson on the Polarization of Radio Galaxies and the Cosmic Microwave Background, *Phys. Lett. B* **289**, 67 (1992).
- [58] E. Witten, Dyons of charge $e\theta/2\pi$, *Phys. Lett. B* **86**, 283 (1979).
- [59] G. Rosenberg and M. Franz, Witten effect in a crystalline topological insulator, *Phys. Rev. B* **82**, 035105 (2010).
- [60] H.-G. Zirnstein and B. Rosenow, Topological magnetoelectric effect: Nonlinear time-reversal-symmetric response, Witten effect, and half-integer quantum Hall effect, *Phys. Status Solidi B* **257**, 1900698 (2020).
- [61] K. Fujikawa, Path-Integral Measure for Gauge-Invariant Fermion Theories, *Phys. Rev. Lett.* **42**, 1195 (1979).
- [62] K. Fujikawa, Path integral for gauge theories with fermions, *Phys. Rev. D* **21**, 2848 (1980).
- [63] D. J. E. Marsh, K. C. Fong, E. W. Lentz, L. Šmejkal, and M. N. Ali, Proposal to Detect Dark Matter Using Axionic Topological Antiferromagnets, *Phys. Rev. Lett.* **123**, 121601 (2019).
- [64] J. Schütte-Engel, D. J. E. Marsh, A. J. Millar, A. Sekine, F. Chadha-Day, S. Hoof, M. N. Ali, K. C. Fong, E. Hardy, and L. Šmejkal, Axion quasiparticles for axion dark matter detection, *J. Cosmol. Astropart. Phys.* **2021**, 066 (2021).
- [65] H. S. Røising, B. Fraser, S. M. Griffin, S. Bandyopadhyay, A. Mahabir, S.-W. Cheong, and A. V. Balatsky, Axion-matter coupling in multiferroics, *Phys. Rev. Res.* **3**, 033236 (2021).
- [66] D. J. E. Marsh, J. I. McDonald, A. J. Millar, and J. Schütte-Engel, Axion detection with phonon-polaritons revisited, *Phys. Rev. D* **107**, 035036 (2023).
- [67] A. M. Shuvaev, G. V. Astakhov, A. Pimenov, C. Brüne, H. Buhmann, and L. W. Molenkamp, Giant Magneto-optical Faraday Effect in HgTe Thin Films in the Terahertz Spectral Range, *Phys. Rev. Lett.* **106**, 107404 (2011).
- [68] L. N. Maurer, J. K. Gamble, L. Tracy, S. Eley, and T.-M. Lu, Designing Nanomagnet Arrays for Topological Nanowires in Silicon, *Phys. Rev. Appl.* **10**, 054071 (2018).
- [69] A. G. Gurevich, *Ferrites at Microwave Frequencies* (Peter Perogrinus Ltd., London, 1987).